Med Biol Eng Comput (2011) 49:1299–1310
DOI 10.1007/s11517-011-0800-9

ORIGINAL ARTICLE

Detection of the intima and media layer thickness of ultrasound common carotid artery image using efficient active contour segmentation technique

N. Santhiyakumari · P. Rajendran · M. Madheswaran · S. Suresh

Received: 24 January 2010 / Accepted: 2 July 2011 / Published online: 20 July 2011

Abstract An active contour segmentation technique for extracting the intima–media layer of the common carotid artery (CCA) ultrasound images employing semiautomatic region of interest identification and speckle reduction techniques is presented in this paper. An attempt has been made to test the ultrasound images of the carotid artery of different subjects with this contour segmentation based on improved dynamic programming method. It is found that the preprocessing of ultrasound images of the CCA with region identification and despeckleing followed by active contour segmentation algorithm can be successfully used in evaluating the intima–media thickness (IMT) of the normal and abnormal subjects. It is also estimated that the segmentation used in this paper results an intermethod error of 0.09 mm and a coefficient of variation of 18.9%, for the despeckled images. The magnitudes of the IMT values have been used to explore the rate of prediction of blockage existing in the cerebrovascular and cardiovascular pathologies and also hypertension and atherosclerosis.

Keywords B-mode ultrasound (US) image · Common carotid artery (CCA) · Active contour (AC) · Improved dynamic programming · Intima–media thickness (IMT)

N. Santhiyakumari (✉)
Department of ECE, K. S. Rangasamy College of Technology, Tiruchengode 637209, India
e-mail: santhiyarajee@rediffmail.com

P. Rajendran
Department of CSE, K. S. Rangasamy College of Technology, Tiruchengode 637209, India
e-mail: peerajendran@gmail.com

M. Madheswaran
Center for Advanced Research, Department of Electronics and Communication Engineering, Muthayammal Engineering College, Rasipuram 637 408, Tamilnadu, India
e-mail: madheswaran.dr@gmail.com

S. Suresh
Director, Mediscan Systems, Diagnostic Ultrasound Research and Training Centre, 197 Dr. Natesan Road, Mylapore 600 004, Chennai, Tamilnadu, India
e-mail: mediscan@gmail.com

1 Introduction

The measurement of various parameters to diagnose the cerebrovascular and cardiovascular pathologies has been shown more attention in the recent past. Earlier studies [3, 25] revealed that measuring intima–media thickness (IMT) in the common carotid artery (CCA) can be used to detect and quantify the progression of atherosclerosis, which may lead to myocardial infarction and stroke [41]. It has been reported that IMT [15] is a good predictor of stroke [11, 47] incidence. It is also a fact that the increase in the IMT of the CCA directly associated with an increased risk of [2, 13, 45] myocardial infarction and stroke, especially in elderly adults [17, 38] without any history of cardiovascular disease. Noninvasive B-mode ultrasound imaging with high resolution is being used to estimate the IMT of the human carotid arteries.

Several studies have been made to improve the estimation of the boundaries of the US images using manual tracing method and found that it is less reproducible and time consuming.

It is not suitable to analyze the large database. The performance depends on the experience of the physicians and hence forced to extract the interesting data from the segmentation of intima–media complex with the help of trained radiologist [7, 9]. Several automatic algorithms have been proposed in order to avoid the manual IMT calculation and manual segmentation of the CCA wall by Kirsch operator [4] and Kalman star algorithm [1]. The segmentation technique was devised to track the progression of ulcerated plaque using balloon modeling technique [8, 16]. Though the technique is proved to be efficient modeling, it has the drawback of identifying the plaque tissues. The counter probability distribution (CPD) functions for entropy mapping and morphological operations [33] have been used for the determination of segmentation but it requires long execution time.

The edge detection techniques reported in papers [20, 31] using region growing and gradient filters were ill suited to detect the local border of the artery due to the stopping criteria problems. The dynamic programming procedure can be used to detect the boundaries of artery [27] considering the approximate location of vessel wall interfaces using optimality principle. Generally, IMT is measured by the skilled operators based on their experience gained from various subjects, just by fixing the markers on the image. This leads in difference in the IMT measurements done by the intra-observer and interobserver as reported elsewhere [48]. It is also found that the user interactions are needed to select a region of interest [18], and in some cases, the radiologists knowledge were required to start the segmentation process [28, 29]. The manual segmentation process is not accepted due to the complexity in the selection of the correct starting point the operator finds difficult to segment the layers with vascular pathologies like increased IMT, plaque and stenosis.

The authors in their earlier work have described a method [39] to segment the near wall of the CCA using dynamic programming method. The authors discussed a method [42] to segment the far wall of the CCA using improved dynamic programming method for normal and abnormal subjects. It overcomes the drawbacks of conventional detection techniques. The authors in their previous work extracted the IM layer, and the thicknesses [43] were measured for the calcified image. A CCA transversal image segmentation technique for identifying the presence of atherosclerosis and analyzing the same for vascular pathologies [44] has been explained by the authors.

In this paper, a reliable extraction technique has been proposed for B-mode US images in the postprocessing steps which do not require any external interaction. The objective of this proposed paper is to develop and to evaluate an IMT after extracting the layers from the CCA image to perform further analysis by utilizing a semiautomatic initialization procedure followed by speckle reduction technique in the preprocessing steps. The AC algorithm utilizes an optimal initial contour technique to extract the corresponding artery boundary. It also utilizes [3, 7, 9, 22, 25, 40, 41] intensity initialization procedure and speckle removal in US images of the carotid artery trying to overcome some of the previous difficulties.

2 Methods

2.1 Carotid artery anatomical structure

The CCA wall consists of three different layers namely an internal tunica (intima), thick layer of transversal muscular tissues (media) and external and more [35] connective layer (adventitia). The intima–media thickness (IMT) is correlated with an augmented risk of severe pathologies. Hence, the analysis of the CCA layers is of important for an effective evaluation of a patient. Near and far walls can be visualized on B-mode scanning, but B-mode evaluation of the near wall is less reliable than the far wall, since far wall has better reflections (high intensity). This is due to the acoustics impedance sequence of the lumen-intima–media-adventitia interface. It has been shown that the measurement of far wall intima–media thickness is reflected by the distance between two edges. Figure 1 shows a carotid artery image and its schematic illustration of echo zones (Z1–Z7) and relevant vessel interfaces (I2, I3, I5, I6) of the near wall and far wall. IMT is defined as the distance between the leading edge of the first echogenic line (lumen-intima interface) and the second echogenic line (media-adventitia interface) of the arterial wall [35], i.e., I2 and I3 for the near wall and I5 and I7 for the far wall [18]. Lumen diameter (LD) is the distance between I3 and I5.

2.2 Active contour segmentation algorithm implementation

Active contour segmentation algorithm for segmentation of the US images is given,

Step1: Image acquisition using ultrasound system.
Step2: Identification of the region of interest.
Step3: Nonlinear filtering to remove speckles in ultrasound images.
Step4: Entropy thresholding for intima layer contour detection.
Step5: Contour initialization for medial layer detection.
Step6: Energy estimation process.
Step7: Evaluation of IMT of various subjects.

2.3 Image acquisition

Philips HD11XE US machine (Model No—HDI5000 sonoct) with the broadband compact linear array transducer has been used for the data acquisition of the images. High definition SonoCT was used to capture real time

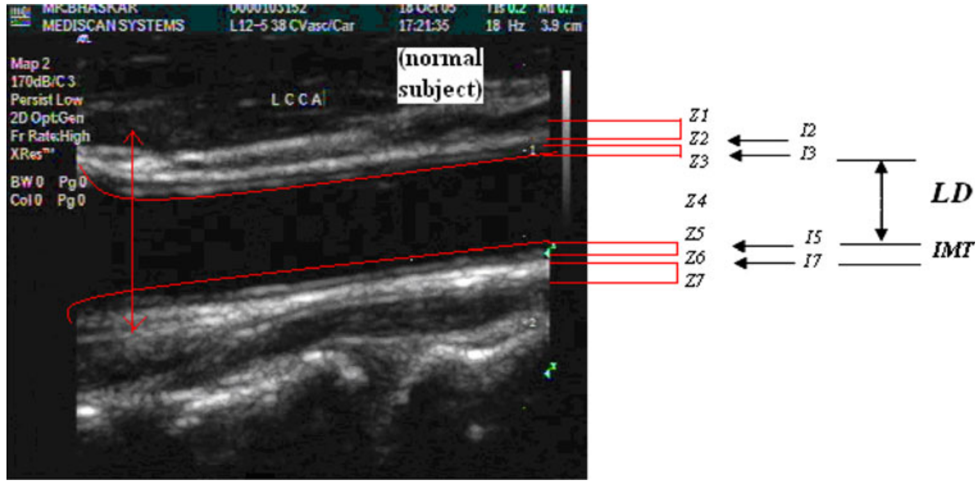

Fig. 1 Carotid artery image of normal subject and definition of echo zones and interfaces

compounded images using transmit beam steering [42]. A multifrequency linear transducer with a frequency range of 7–15 MHz has been used for recording the arterial movements. The transducer is operated at a frequency of 12 MHz to obtain the arterial movements, and the movements are recorded using video recorder. One can identify the exact transducer position (at right angles to adventitia) by placing at different inclined angles. The video is recorded for a period of 10 s for each subject to show the longitudinal sections of the CCA.

To obtain an uniform lumen for different subjects, the transducer is placed exactly at the starting point of the bifurcation of CCA. Thus, the left end of the image indicates the starting point of bifurcation. The recorded video is converted into frames employing OSS video decompiler. The converted frames are stored as still images in a PC for further processing. Thus, the above images have been used to measure the IMT of CCA employing AC technique. In order to obtain the natural flow of lumen during systolic and diastolic pressure, the video has been recorded for 10 s. The still images obtained from 10 s video consist of approximately 180 frames which reflect the changes in the magnitude of vascular wall during systolic and diastolic operations. Therefore, the IMT has been measured in all 180 images, and the average value has been used for further analysis. IMT measurements have been carried out at 30 points from the identified region of the far wall CCA.

2.4 Identification of the region of interest (ROI)

The procedure is devised to have less operator dependence. The first stage of the algorithm is the identification of the portion of the image where the CCA region is located. Parameters pertaining to the vessel lumen and the adventitia have been considered to identify CCA region correctly. The lumen is characterized by pixels with low intensity and relatively low variance (low US echoes of the blood cells and relative homogeneity of the medium) and surrounded by high-intensity pixels belonging to the carotid walls. This feature is used to identify the CCA region very precisely. Hence, for each and every pixel in the image, the mean intensity and variance are measured using NXN square neighborhood ($N = 10$ is utilized in this work). In CCA US vascular images, the adventitia is characterized by a high value of pixel intensity due to its higher acoustic impedance.

This can be carried out by estimating the intensity profile for each pixel and calculating the mean for detecting edges of various layers. The pixel with local maximum intensity has been considered as pixel with adventitia. Similarly, pixel with local minimum intensity has been treated as pixel with lumen in arterial layers.

2.5 Image initialization procedure

In order to measure the thickness of the intima–media layer, the identified ROI is further processed by selecting the upper left and lower right vertexes. The points are denoted as $P_1(x_1, y_1)$ and $P_2(x_2, y_2)$. Finally, the layers have been detected by applying an active contour segmentation procedure.

2.6 Speckle reduction

The preprocessing steps have been used to remove the speckles without disturbing any important features. The obtained ultrasound speckle noise has a logarithmic compressed Rayleigh distribution. It can be noted that the ultrasound speckle noise follows the Rayleigh distribution and can be modeled with zero mean Gaussian variable having standard deviation σn [12, 14, 23]. Hence, in this paper, the first step is to model the speckle noise with Rayleigh distribution as Gaussian variable with zero mean. The following Eq. (1) is used to model the acquired image as.

$$I_O = I + I_O = I + \sqrt{\mathrm{IN}} \quad (1)$$

where I_o is the observed image, I is the initialized image, and N is the Gaussian variable with zero mean [5]. The modeled images have been despeckled using speckle reducing anisotropic diffusion method (SRAD). SRAD [47] method has been used to enhance the edges by inhibiting diffusion across edges and allowing diffusion on either side of the edge. Speckle smoothing is carried out by considering an intensity image $I_o(x, y)$. The output image $I(x, y: t)$ has been evaluated using the following (PDE) partial derivative equation.

$$\begin{gathered} \mathrm{d}I(x,y;t)/\mathrm{d}t = \mathrm{div}[c(q)\nabla \mathrm{I}(x,y:t)] \\ I(x,y;0) = I_0(x,y).(\partial I(x,y)/\partial \vec{\mathrm{n}})|\partial\Omega = 0 \end{gathered} \quad (2)$$

where $\partial\Omega$ denotes the border of Ω, $\vec{n}$ is the outer normal to the $\partial\Omega$. Equation (2) represents the SRADPDE, and the value c(q) has been estimated using (3) (or) (4).

$$c(q) = \frac{1}{1 + [q^2(x,y:t) - q_0^2(t)]/[q_0^2(t)(1+q_0^2(t))]} \quad (3)$$

(or)

$$c(q) = \exp\{-[q^2(x,y;t) - q0^2(t)]/[q0^2(t)(1+q0^2(t))]\} \quad (4)$$

In (3) and (4), $q(x, y: t)$ is the instantaneous coefficient of variation. Its value has been determined using (5). It has been served as the edge detector for the speckled images and

$$q(x,y:t) = \sqrt{\frac{(1/2)(|\nabla \mathrm{I}|/I)^2 - (1/4^2)(\nabla^2 \mathrm{I}/I)^2}{[1+(1/4)(\nabla^2 I/I)]^2}} \quad (5)$$

$q_o(t)$ is the speckle scale function, and it has been used effectively to control the amount of smoothing applied to the image by SRAD. Its value is estimated using (6).

$$\mathrm{qo}(t) = \frac{\sqrt{\mathrm{var}[\mathrm{Z(t)}]}}{\overline{z(t)}} \quad (6)$$

where var $[Z(t)]$ and $\overline{Z(t)}$ are the intensity variance and mean over a homogeneous area at t. This SRADPDE is preferred since it exploits the instantaneous coefficient of variation in reducing speckle and provides superior performance over conventional anisotropic diffusion method in terms of smoothing uniform regions and preserving edges and features.

2.7 Intima layer contour detection procedure

The contour of the intima layer from the SRAD images has been detected using the entropy thresholding technique [5, 19, 37]. The following procedure has been used for the intima layer detection.

Step1: Initial line has been set in the upper edge (left top most corner in the segmented region) of the despeckled ROI image.
Step2: The points in the line have been mentioned as p_1, $p_2,\ldots,p_C$.
Step3: The point has been chosen as unfrozen point $P \equiv (x, y)$ at the spatial beginning of the left top most corner of the segmented region.
Step4: The point is considered as frozen in the line if the value of $|\nabla \mathrm{I}(p)| \geq \mu \mathrm{Tg}$ where μ is a constant and its value has been measured after several iterations as 0.73, and Tg is a threshold of the image. Its value has been calculated from the histogram gradient of ROI $(|\nabla \mathrm{IROI}(x,y)|)$ through the entropy threshold method.
Step5: The point P has been fixed at the position if one of the neighbors of P is frozen with higher gradient between $(x, y-1)$, (x, y) and $(x, y + 1)$, this step has been followed by step 7.
Step6: The point has been moved to$(x, y + 1)$.
Step7: If all the points are fixed, then the steps have been terminated.
Step8: If all the points are not fixed, then the step 3 has been followed.

2.8 Medial layer contour detection procedure

An active contour segmentation procedure implemented in this study is based on the initial contour selection and energy minimization process. After the intimal layer detection, the initial contour has been created using the point $P_1(x_1, y_1)$. Before the algorithm has been proceeded, the following characteristics of an edge are considered, i.e., an edge is characterized both by change in intensity of a pixel $(|\nabla \mathrm{I}(x,y)|)$ and the position of a pixel from the origin to the vertical axis, i.e., $\mathrm{Iy}(x, y)$. Therefore, to identify an adventitia edge point, the following function has been used $(|\nabla \mathrm{I}(x,y)| + \mathrm{Iy}(x,y))^2$. The following steps have been used to calculate the chain of points in a line.

Step1: The point L_0 has been set as $L_1 = P_1(x_1, y_1)$.
Step2: For each and every point (i.e., L2, L3,…, Lc) in a line, the location has been searched as $L_i = L_{i-1}(x_{i-1} + 1, y_{i-1} + j)$ with $j = -1, 0, 1$, where the function $(|\nabla \mathrm{I(Li)}| + \mathrm{Iy(Li)})^2$ has higher value and $L_i(x_i, y_i)$ satisfies the condition as $L_i(x_i, y_{i\text{-}S}) = p_i(x_i, y_i)$ where $s \geq$ distance.

The effect of the intima layer is null in the energy minimization process, since the value for a distance is a constant and this value has been considered as the intima thickness. The initial contour defined by the previous process avoids the multiple contour and it guarantees a fast convergence in the minimization process. In this way, the

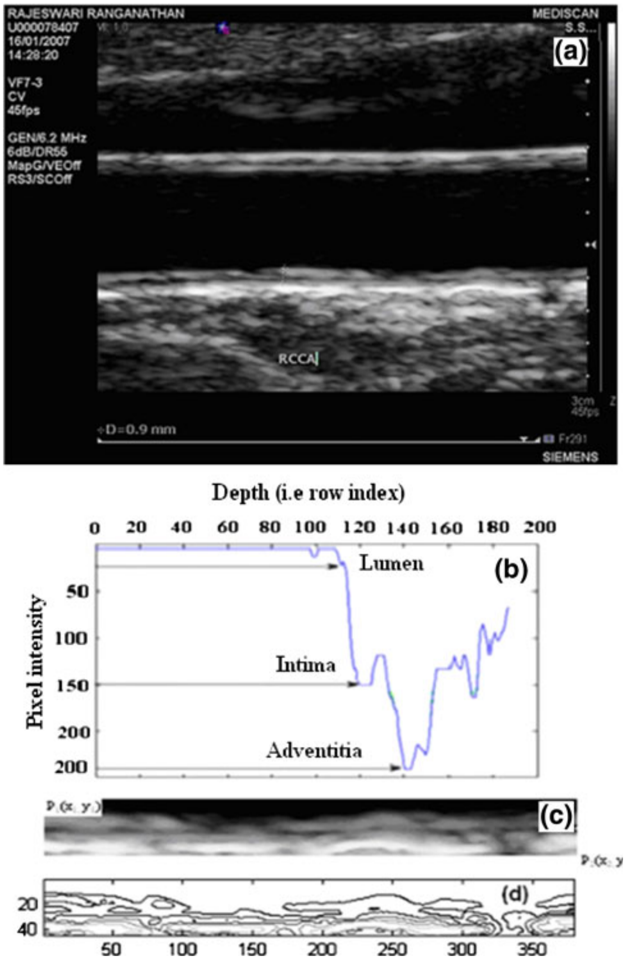

Fig. 2 **a** Common carotid artery hypertension subject sample frame showing longitudinal section. **b** Pixel intensity versus depth (i.e., row index), corresponding to a column of a sample image. **c** Initialized ROI image of hypertension subject. **d** SRAD image with intimal contour of hypertension subject

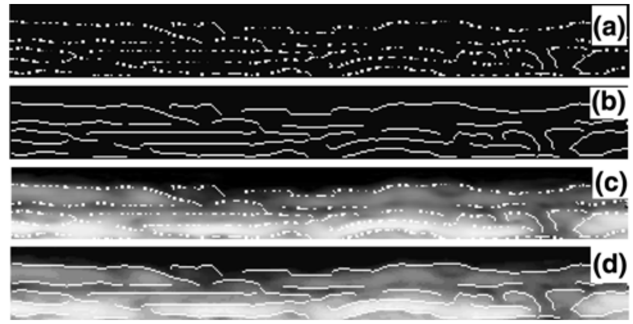

Fig. 3 **a** External energy of ROI image of hypertension subject. **b** Total energy of ROI image of hypertension subject. **c** Segmented region of hypertension subject using external energy. **d** Segmented region of hypertension subject using total energy

energy minimization process has not been affected by the intimal edge attraction.

2.8.1 Energy minimization process

An active contour is a parametric contour and it is a curve [48] which has been represented by a two-dimensional function as $X(s) = [x(s), y(s)]$, where $(x, y) \in R^2$ denotes the spatial coordinates of an image and $s \in [0, 1]$ represents the parametric domain. The energy functional has been defined by the following term E, and it is represented in (7).

$$E = \int_0^1 \frac{1}{2}\left[\alpha|X'(s)|^2 + \beta|X''(s)|^2\right] + \mathrm{Eext}(X(s))ds \tag{7}$$

where α and β are the weighting parameters which controls the active contour continuity and smoothness and rigidity, $X'(s)$ and $X''(s)$ are the first and second order derivatives of

Table 1 Intima–media thickness of common carotid artery for different age groups of normal (healthy) subjects

S. No.	1	2	3	4	5
Age group (years)	21–30	31–40	41–50	51–60	61–70
Number of subjects	15	13	16	13	06
Male/female	M	F	M	F	M
AC method					
$IMT_{Max\ +\ SD}$ (mm)	0.32 ± 0.03	0.41 ± 0.01	0.47 ± 0.02	0.55 ± 0.01	0.60 ± 0.02
$IMT_{Min\pm\ SD}$ (mm)	0.24 ± 0.07	0.39 ± 0.02	0.45 ± 0.02	0.53 ± 0.01	0.57 ± 0.01
$IMT_{mean\ \pm\ SD}$ (mm)	0.28 ± 0.05	0.41 ± 0.02	0.47 ± 0.01	0.54 ± 0.01	0.59 ± 0.02
DP method					
$IMT_{Max\ \pm\ SD}$ (mm)	0.42 ± 0.029	0.59 ± 0.006	0.52 ± 0.018	0.65 ± 0.003	0.70 ± 0.024
$IMT_{Min\pm\ SD}$ (mm)	0.34 ± 0.065	0.49 ± 0.018	0.55 ± 0.016	0.63 ± 0.006	0.67 ± 0.007
$IMT_{mean\ \pm\ SD}$ (mm)	0.38 ± 0.047	0.51 ± 0.018	0.57 ± 0.011	0.64 ± 0.005	0.69 ± 0.016
Inter method error S (mm)	0.097	0.09	0.10	0.10	0.096
Coefficient of variation CV (%)	25.63	18.9	18.87	17	15

According to the literature [26], it has been seen that the IMT is supposed to be 0.2 to 0.3 mm for 20 to 30 years, 0.4 to 0.5 mm for 40 to 50 years, 0.6 to 0.7 mm for 60 to 70 years

$x(s)$ with respect to s. The external energy function E_{ext} values have been taken from the image which has the features of interest such as boundaries. The E_{ext} functional has been defined by the (8) and (9) as

$$\mathrm{E}^{(1)}\mathrm{ext}(x,y) = -|\nabla \mathrm{I}(x,y)|^2 \tag{8}$$

$$\mathrm{E}^{(2)}\mathrm{ext}(x,y) = -|\nabla[\mathrm{G}\sigma\mathrm{G}\sigma(y)^{*}I(x,y))]^2| \tag{9}$$

where $\mathrm{G}_{\sigma}(x,\ y)$ is a two-dimensional Gaussian function with standard deviation σ, and $\nabla$is the gradient operator. Large value of $\boldsymbol{\sigma}$ has been taken, since this large value makes the boundary to be blurry one. The capture range of the active contour has been increased by energy minimization process which satisfies the following Euler equation. It is denoted in (10). This Euler expression can be represented as a force balance equation and is shown in (11).

$$\alpha \mathrm{X}''(\mathrm{s}) - \beta \mathrm{X}''''(\mathrm{s}) - \nabla \mathrm{Eext} = 0 \tag{10}$$

$$\mathrm{Fint} + \mathrm{F}^{(\mathrm{p})}\mathrm{ext} = 0 \tag{11}$$

where $\mathrm{Fint} = \alpha \mathrm{X}''(\mathrm{s}) - \beta \mathrm{X}''''(\mathrm{s})$ and $\mathrm{F}^{(\mathrm{p})}\mathrm{ext} = -\nabla \mathrm{Eext}$. The values for the term $\alpha = 0.55$ and $\beta = 0.43$ have been

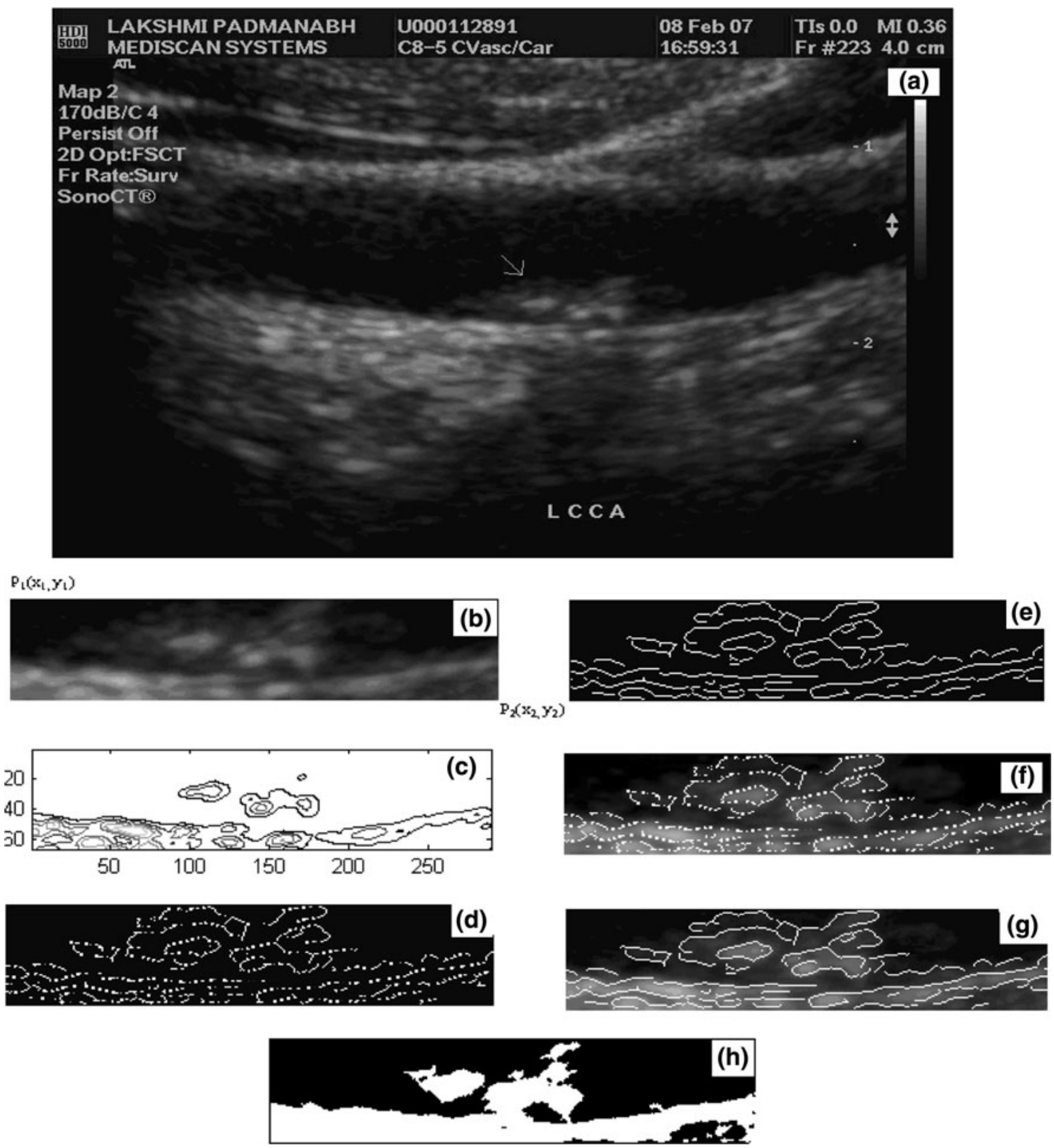

Fig. 4 **a** Common carotid artery atherosclerosis subject. **b** Initialized ROI image of atherosclerosis subject. **c** SRAD image with intimal contour of atherosclerosis subject. **d** External energy of ROI image of atherosclerosis subject. **e** Total energy of ROI image of atherosclerosis subject. **f** Segmented region of atherosclerosis subject using external energy. **g** Segmented region of atherosclerosis subject using total energy. **h** Entropy threshold image

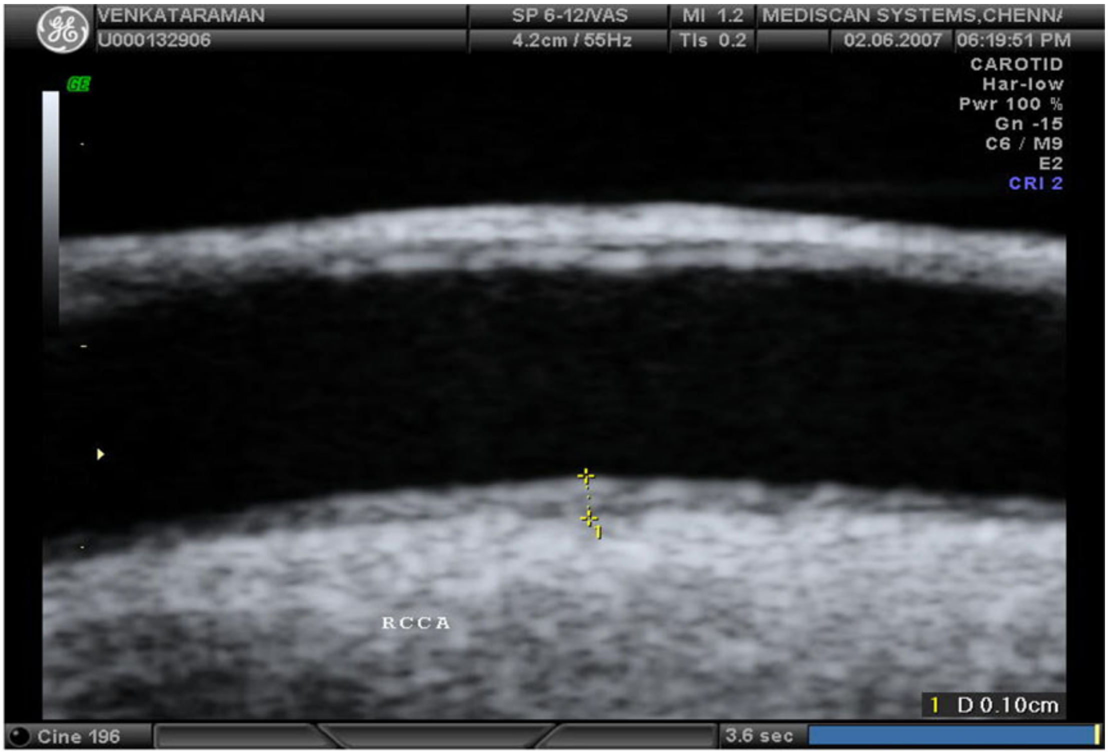

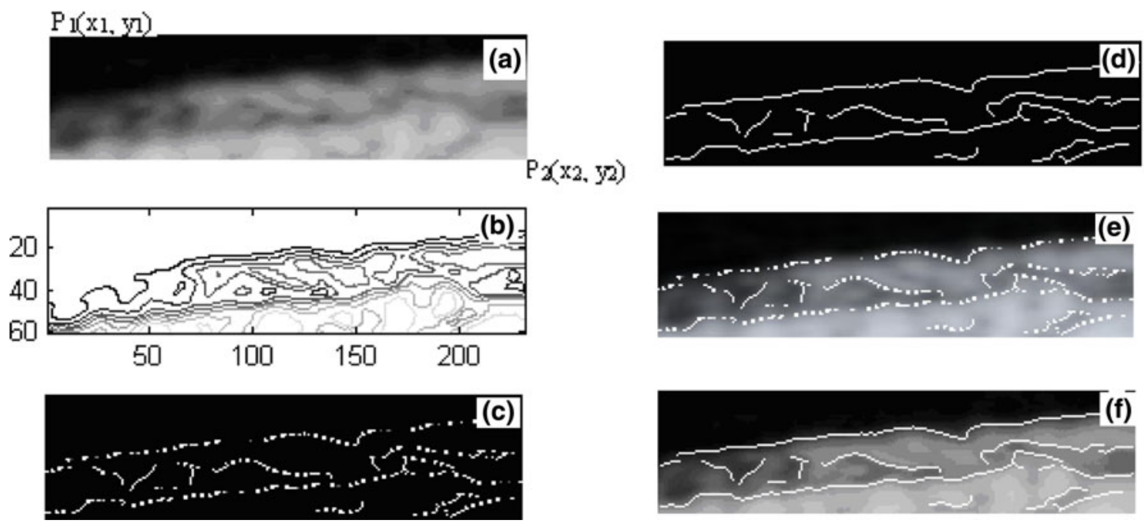

Fig. 5 Common carotid artery diabetes subject. **a** Initialized ROI image of diabetes subject. **b** SRAD image with intimal contour of diabetes subject. **c** External energy of ROI image of diabetes subject. **d** Total energy of ROI image of diabetes subject. **e** Segmented region of diabetes subject using external energy. **f** Segmented region of diabetes subject using total energy

used in this work. The continuity and smoothness of the contour have been discouraged by the internal force. The active contour toward the desired image edges has been pulled by the external force.

2.9 Univariate statistical analysis

In order to evaluate how the results of the active contour segmentation method differ from the improved dynamic programming method, the following metrics have been used in this analysis. The parameters $IMT_{mean,}$ IMT_{max} and IMT_{min} as well as the intermethod error [6] according to the formula $\mathbf{S = SD_{IMT}}/\sqrt{2}$, with SD_{IMT}, the standard deviation for each of the 100 subjects have been measured. The coefficient of variation CV% has been calculated, which describes the difference as a percentage of the pooled mean value with $\mathbf{CV\% = (S\ .100)}/\overline{\mathrm{IMTmean}}$ [6] where $\overline{\mathrm{IMTmean}}$ is the pooled mean value. The Wilcoxon matched pairs rank sum test is used to identify a significant difference exists between all the segmented boundaries for each set of measurements, at $P < 0.001$. The association between the active contour and improved dynamic programming measures is characterized by using Pearson's correlation coefficient (ρ).

3 Results

Common carotid artery images are acquired from the US scanner, and the segmentation procedure mentioned in the previous paragraph has been applied. For the present analysis, 100 subjects have been acquired, out of which 63 subjects were both male and female with age varying from 20 to 70 years. In this study, only 63 subjects have been considered with healthy nature and without a personal or family history of cerebrovascular and cardiovascular pathologies. Remaining 37 subjects have abnormalities like diabetes, hypertension and atherosclerosis. Sample of longitudinal section B-mode image with hypertension subject is shown in Fig. 2a. Figure 2b shows the pixel intensity profile for the longitudinal section. This profile is used to locate the lumen-intima interfaces and adventitia-media interfaces in an overall tissues. It can be seen that the adventitia tunica corresponds to the global maximum and its pixel intensity value has 240, whereas the carotid tunica media and tunica intima corresponds to the less intensity portion ranges from 150 to 240 and the carotid lumen corresponds to very low intensity of 20 in the intensity profile.

Figure 2c represents the initialized ROI image with the starting and ending point as P1($x1$, $y1$) and P2($x2$, $y2$) in the upper left and lower right vertex of ROI. The speckles present in the US images have been removed using SRADPDE techniques, and its despeckled image with contours is shown in Fig. 2d. It is obtained using entropy thresholding technique with Tg = 64. The intimal and adventitial layer contours are clearly viewed in the external and total energy of SRAD images as in Fig. 3a and b. The contours have been extracted using the energy minimization process is superimposed with the initialized image, and the resultant images are shown in Fig. 3c and d. The layer continuation is very clear in Fig. 3d as compared to Fig. 3c since the weighting parameters α and β maintain the smoothness and rigidity in a controlled way as compared to the external energy of an image. From the extracted boundary layers of intima and media of the artery, the evaluations are made in upward and downward directions.

The frames are taken for about 2–3 cardiac cycles. The view of the extracted far wall layer boundaries for the hypertension subject under longitudinal B-mode frames is shown, respectively, in Fig. 3d. The above procedure is applied to all the 63 subjects with age group varying from 20 to 70 years. As a first step, measurements have been made on the healthy subjects (free from diabetes and atherosclerosis). The IMT is estimated considering all the age groups with normal subjects are presented in Table 1.

This is done for a series of consecutive frames obtained from the video image of a single subject. The same procedure is applied to 37 subjects with abnormalities like diabetes,

The same procedure is applied to 37 subjects with abnormalities like diabetes, hypertension and atherosclerosis, and its results are shown in Fig. 3 for the subjects with hypertension. Similar results have been obtained for the subjects with atherosclerosis and diabetes subjects. These results are shown in Figs. 4 and 5. The IMT is estimated, and its values are presented in Table 2. After extracting the far wall layers, the IMT is evaluated considering the distances between the upper and lower boundary lines. The IMT is estimated in longitudinal frames considering 20 to 40 points. The locations of the artery wall with columns of a single subject are viewed in the graph.

Figure 6 shows the segmented region of diseased subjects. The IMT of the hypertension subject is evaluated as 2 mm for an age of 58 is calculated by pixel distance between the low intensity value and high intensity value of the CCA, and the same is shown in Fig. 7a. The graph is

Table 2 Intima–media thickness of common carotid artery for abnormal subjects like hypertension and atherosclerosis

S. No.	1	2	3
Age group (years)	40–75	40–75	40–75
Number of subjects	15	13	09
Name of the pathology	Hypertension	Atherosclerosis	Diabetes
DP method			
$IMT_{mean \pm SD}$ (mm)	2.02 ± 0.12	3.85 ± 0.01	2.85 ± 0.02
AC method			
$IMT_{mean \pm SD}$ (mm)	2.01 ± 0.04	3.35 ± 0.41	2.75 ± 0.02
Intermethod error S (mm)	0.09	0.10	0.10
Coefficient of variation CV (%)	6.186	2.624	3.546
Pearson's correlation coefficient (ρ)	**0.94**	**0. 974**	**0.965**

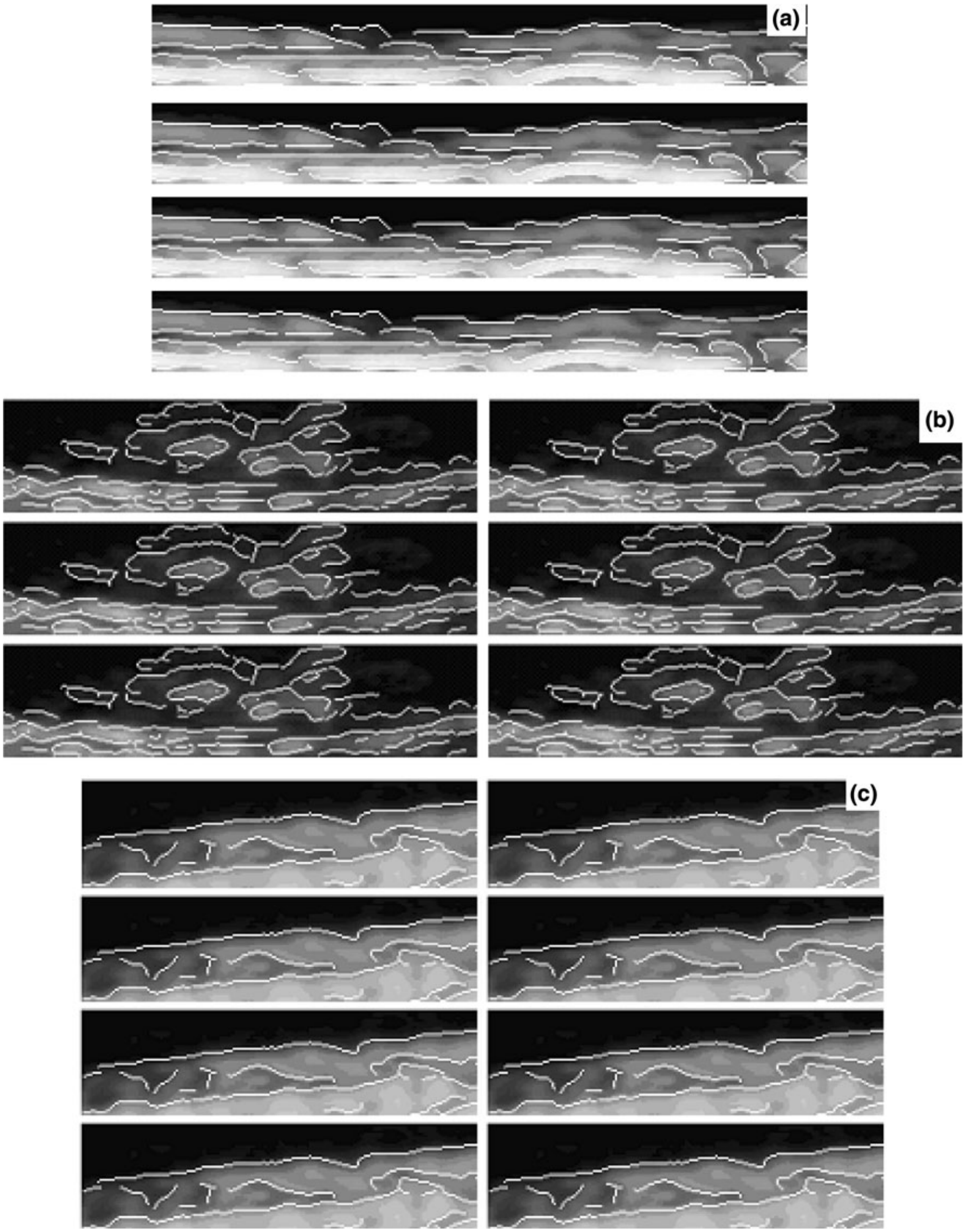

Fig. 6 **a** IMT segmented region of hypertension subjects. **b** IMT segmented region of atherosclerosis subjects. **c** IMT segmented region of diabetes subjects

shown for a single subject with an age of 58 years. The observed results for the age group of 40–75 are shown in Table 2.

Similarly, the IMT of the diabetes subject is evaluated as 2.76 mm for an age of 72 is calculated by pixel distance between the low intensity value and high intensity value of the CCA, and the same is shown in Fig. 7b. The graph is shown for a 72 years. Figure 8 shows the Bland–Altman plots for the proposed method with the manual method. These results have been validated by medical experts [34, 40, 46].

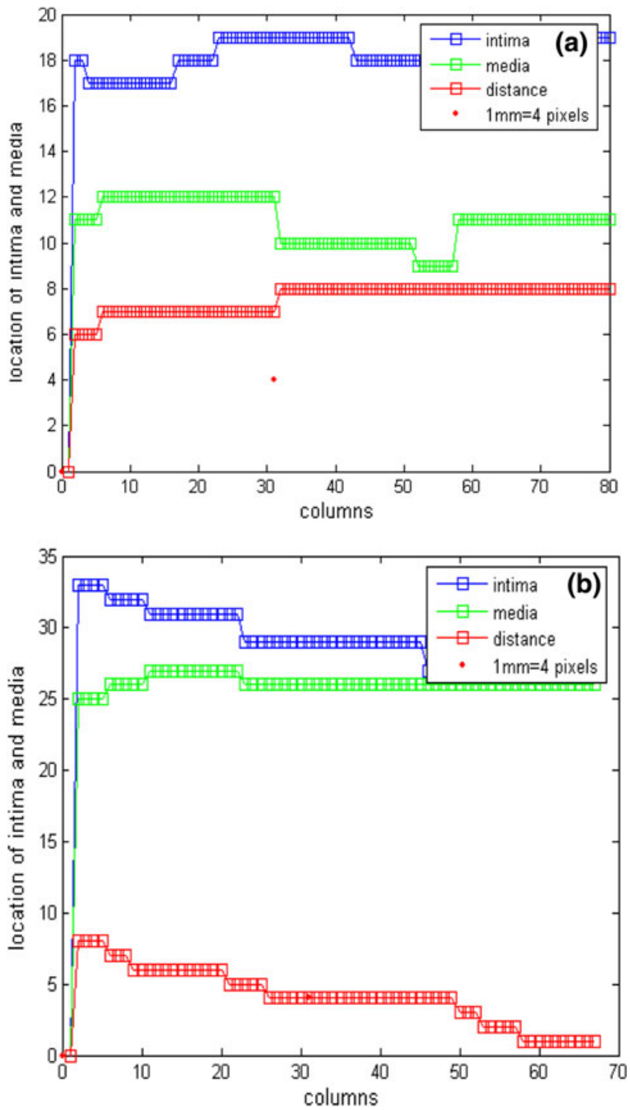

Fig. 7 **a** IMT graph of hypertension subject. **b** IMT graph of diabetes subject

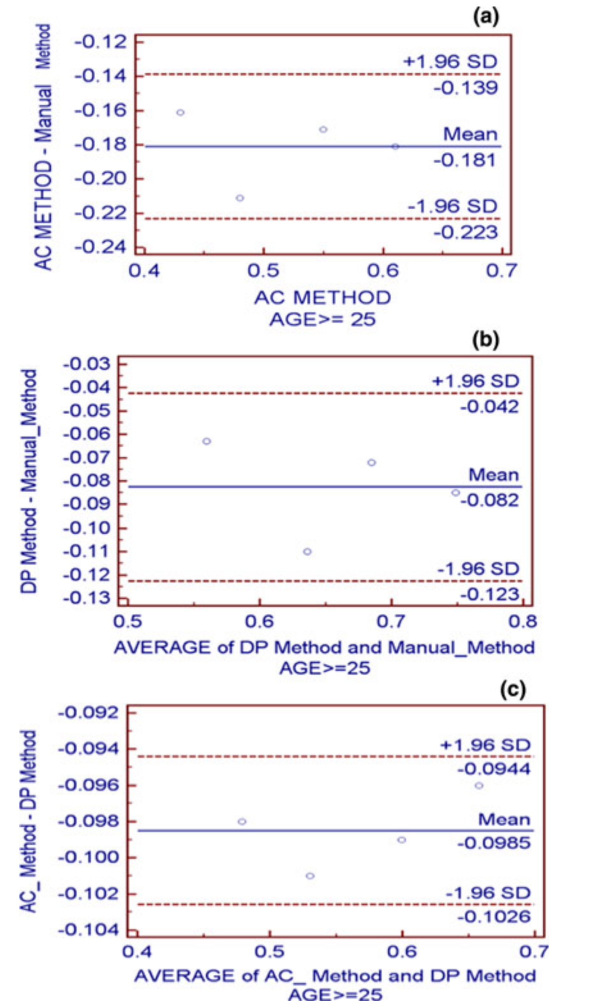

Fig. 8 **a** Bland–Altman plot for AC method versus manual method. **b** Bland–Altman plot for DP method versus manual method. **c** Bland–Altman plot for AC method versus DP method

4 Discussion

The objective of this paper was to extract an intima–media layer and to evaluate an IMT of CCA using active contour segmentation method. It also utilizes a region of interest identification and speckle reduction in US of CCA. The proposed technique overcomes the difficulties of conventional detection techniques. The thicknesses of layers were measured for 63 normal as well 37 abnormal objects. Furthermore, to investigate under what condition the AC segmentation measurements are closer and better to an improved dynamic programming method. The study showed that in Table 1, the IMT increases for higher age group people. The observed results can be used to determine the morphological changes in the layers which lead to blockage in the subjects in very earlier stages in the near future. The results shown in Figs. 4 and 5 indicate that the distance between the extracted layers is larger than the normal subject extracted layers.

The graph shown in Fig. 7a and b gives an idea about the thickness of the vessel based on the evaluated distance between the locations of the interfaces. This distance is a measure of length of the column in the intensity distribution profile of the image. All the points in the location of the interfaces along the columns are considered for the evaluation, and it has been shown that 1 mm is approximately equal to 4 pixels for longitudinal sections of CCA. The observed results for the age group of 40–75 are shown in Table 2. The evaluated IMT for the abnormal subject differs much as compared to normal subject, since intima and media layers gap is much wider. From the evaluated results as in Table 2, it is inferred that the subject with atherosclerosis, diabetes and hypertension has higher layer thickness as compared to the normal subject. It can be seen that IMT increases even for middle age group people with abnormalities.

At the same time, the subject with diabetes has much higher thickness as compared with the hypertension subject, and it is clearly viewed in Fig. 5f. The obtained results indicate the presence of calcification in the segmented region. The region with the calcification has been segmented and is shown in Fig. 4g. It has been observed from the segmented results that the layers extracted using proposed technique provide accurate results as compared to improved dynamic programming method. It has been seen from the literature [28] that the IMT for the normal patient with an age between 21 and 30 is estimated as 0.2 to 0.3 mm. From this, it is concluded that the AC technique provided the results close to the results given by [28]. AC technique is an efficient one since it performs the computation in a faster way and requires moderate effort to write the software. The algorithms resulted in more accurate. The occurrence of wrong detection is so rare and be considered insignificant. It is the better method accounts for the continuity of the detected boundaries. The segmented results are in line with the earlier studies [10, 11, 15, 17, 21, 33, 41, 47].

It is evident from the above observations that the IMT linearly increases as age increases. This is due to the reduction in the circumference of the vascular tube which leads to early prediction of blockage which causes the cerebrovascular and cardiovascular pathologies. The observed increase in the IMT magnitude for the subjects like hypertension and atherosclerosis is ascribed due to the deposition of calcification (or) plaque. The observed results are in line with the earlier studies [3, 7, 17, 25, 33].

In conclusion that the evaluation using active contour segmentation gives better result as compared to improved dynamic programming technique. It is also observed that the IMT linearly increases as age increases which may be due to the reduction in the circumference of the vascular tube which leads to early prediction of blockage which causes the cerebrovascular and cardiovascular pathologies. The present studies confirm that the AC technique can be successfully employed to reveal the early prediction of calcification or plaque.

Acknowledgments The authors would like to express their gratitude to the Management and Ms.Chandra Ganesh, Sonographer, Mediscan systems, Chennai for providing the necessary images for this study.

References

1. Abolmaesumi P, Sirouspour M.R, Salcudean S.E (2000) Real-time extraction of carotid artery contours from ultrasound images. Comput Based Med Syst 181–186
2. Baldassarre D, Amato M, Bondioli A (2000) Carotid artery intima- media thickness measured by ultrasonography in normal clinical practice correlates well with atherosclerosis risk factors. Stroke 31:2426–2430
3. Bots ML, Hoes AW, Koudstaal PJ, Hofman A, Grobbee DE (1997) Common carotid intima—media thickness and risk of stroke and myocardial infarction: the Rotterdam Study. Circulation 96:1432–1437
4. Bottalico MA, Starita A (2000) EcoStudio: a computer tool to support carotid ultrasound images analysis. IEEE Eng Med Biol 4:2428–2430
5. Ceccarelli M, Luca N. De, Morganella A (2006) An active contour approach to automatic detection of the intima-media thickness. In: Proceedings of international conference acoustics, speech and signal processing, vol 2. pp 709–712
6. Chalana V, Kim Y (1997) A methodology for evaluation of boundary detection algorithms on medical images. IEEE Trans Med Imaging 16(5):642–652
7. Chan RC, Khaufhold J, Hemphill LC, Lees RS, Karl WC (2000) Anisotropic edge-preserving smoothing in carotid B-mode ultrasound for improved segmentation and intima-media thickness (IMT) measurement. Comput Cardiol 27:37–40
8. Chen Y, Medioni G (1995) Description of complex objects from multiple range images. IEEE Comput Vision Imag Underst 61(3): 325–334
9. Cheng D, Schmidt-Trucksass A, Cheng K, Burkhardt H (2002) Using snakes to detect the intimal and adventitial layers of the common carotid artery wall in sonographic images. Comput Methods Programs Biomed 67:27–37
10. Cinthio M, Jansson T, Eriksson A, Ahlgren AR, Persson HW, Lindström K (2010) Evaluation of an algorithm for arterial lumen diameter measurements by means of ultrasound. Med Biol Eng Comput 48(11):1133–40. PMID: 20635222
11. Cupini LM, Pasqualetti P, Diomedi M (2002) Carotid artery intima-media thickness and lacunar versus nonlacunar infarcts. Stroke 33:689–694
12. Dh LO, Polak JF, RA Kronmal (1999) Carotid-artery intima and media thickness as a risk factor for myocardial infarction and stroke in older adults. N Engl J Med 340:14–22
13. Dutt V (1996) Adaptive speckle reduction filter for log compressed B-scan images. IEEE Trans Med Imaging 15(6):802–813
14. Ebrahim S, Papacosta O, Whincup P (1999) Carotid plaque, intima media thickness, cardiovascular risk factors and prevalent cardiovascular disease in men and women: the British regional heart study. Stroke 30:841–850
15. Gill JD, Ladak HM, Steinman DA, Fenster A (2000) accuracy and variability assessment of semi-automatic technique for segmentation of the carotid arteries from 3D ultrasound images. Med Phys 27(6):1333–1342
16. Grobbee DE, Bots ML (1994) Carotid artery intima-media thickness as an indicator of generalized atherosclerosis. J Int Med 236:567–573
17. Gustavsson T, Abu-Gharbieh R, Hamameh G, Liang Q (1997) Implementation and comparison of four different boundary detection algorithms for quantitative ultrasonic measurements of the human carotid artery. IEEE Comput Cardiol 24:69–72
18. Haddon JF, Boyce JF (1990) Image segmentation by unifying region and boundary information. IEEE Trans Pattern Anal Mach Intell 12(10):929–948
19. Herrington D, Santago P, Joinson T (1991) Image processing and display of 3D intra-coronary ultrasound images. Comput Cardiol 349–352
20. Jegelevičius D, Lukoševičius A (2002) Ultrasonic measurements of human carotid artery wall intima-media thickness. Ultragarsas 43–47
21. Jin D, Wang Y (2007) Doppler ultrasound wall removal based on the spatial correlation of wavelet coefficients. Med Biol Eng Comput. 45(11):1105–11. PMID: 17684782

22. Krissian K (2004) Anisotropic diffusion of ultrasound constrained by speckle noise model. Technical report. Harvard Medical school
23. Krissian K, Vosburgh K, Kikinis R, Carl-Fredrik Westin (2004) Anisotropic diffusion of ultrasound constrained by speckle noise model. Lab. Math Imaging 1–10
24. Lamont D, Parker L, White M, Unwin N (2000) Risk of cardiovascular disease measured by carotid intima-media thickness at age 49–51: life course study. BMJ 320:273–278
25. Liang Q, Wendelhag I, Wikstrand J, Gustavsson T (2000) A multiscale dynamic programming procedure for boundary detection in ultrasonic artery images. IEEE Trans Med Imaging 19:127–142
26. Liguori C, Paolillo A, Pietrosanto A (2001) An automatic measurement system for the evaluation of carotid intima-media thickness. IEEE Trans Instrum Meas 50(6):1684–1691
27. Liguori C, Paolillo A, Pietrosant A (2001) An automatic measurement system for the evaluation of carotid intima-media thickness. IEEE Trans Instrum Meas 50:1684–1691
28. Loizou CP, Pattichis CS, Pantziaris M, Tyllis T, Nicolaides A (2007) Snakes based segmentation of the common carotid artery intima media. Med Biolo Eng Comput 45(1):35–49
29. Mao F, Gill J, Downey D, Fenster A (2000) Segmentation of carotid artery in ultrasound images: method development and evaluation technique. Med Phys 27(8):1961–1970
30. Molinari F, Rajendra Acharya U, Zeng G, Meiburger KM, Suri JS (2011) Completely automated robust edge snapper for carotid ultrasound IMT measurement on a multi-institutional database of 300 images. Med Biol Eng Comput 2011 Apr 21. [Epub ahead of print] PMID: 21509593
31. Santhiyakumari. N, Rajendran. P, Madheswaran M (2010) Medical decision-making system of ultrasound carotid artery intima–media thickness using neural networks. J Digit Imaging. doi:10.1007/s10278-010-9356-8. Published Online First™, 23 December 2010
32. Pignoli P, Tremoli E, Poli A, Paoletti A (1986) Intimal plus medial thickness of the arterial wall: a direct measurement with ultrasound imaging. Circulation 74:1399–1406
33. Polat K, Latifoglu F, Kara S, Günes S (2008) Usage of a novel, similarity-based weighting method to diagnose atherosclerosis from carotid artery Doppler signals. Med Biol Eng Comput 46(4):353–362
34. Sahoo PK, Soltani S, Wong KC, Chen YC (1988) A survey of thresholding techniques. Comput Vision, Graphics, and Image Process 41:233–260
35. Salonen JT, Salonen R (1993) Ultrasound B-mode imaging in observational studies of atherosclerotic progression. Circulation 87(II):1156–1165
36. Santhiyakumari N, Madheswaran M (2006) Estimation of layer thickness of arterio carotis using dynamic programming procedure. In: Proceedings of 3rd cairo international biomedical engineering conference. IP2, vol 4. pp 1–4
37. Santhiyakumari N, Madheswaran M (2008) Non-Invasive evaluation of carotid artery wall thickness using Improved dynamic programming technique. Signal, Image and Video Process J (Springer) 2:183–193
38. Santhiyakumari N, Madheswran M (2007) Extraction of intima-media layer of arteria- carotis and evaluation of its thickness using active contour approach. In: Proceedings of international conference on intelligent and advanced systems. IP_MS1 582-586
39. Santhiyakumari N, Madheswran M (2009) Analysis of atherosclerosis for identification of cerebrovascular and cardiovascular diseases using active contour segmentation of carotid artery. Int J Bio Med Eng Consumer Health Inform 1(2):121–125
40. SAR Hernandez, Kroon AA, MPJ Van Boxtel (2003) Is there a side predilection for cerebrovascular disease? Hypertension 42:56–60
41. Seçil M, Altay C, Gülcü A, Çeçe H, Göktay AY, Dicle O (2005) Automated measurement of intima-media thickness of carotid arteries in ultrasonography by computer software. Diagn Interv Radiol 11:105–108
42. Veller MG, Fisher CM, Nicolaides AN (1993) Measurement of the ultrasonic intima-media complex thickness in normal subjects. J Vasc Surg 17(7):19–25
43. Wendelhag I, Liang Q, Gustavsson T, Wikstrand J (1997) A new automated computerized analysing system simplifies reading and reduces the variability in ultrasound measurement of intima media thickness. Stroke 28:2195–2200
44. Wilhjelm JE, Gronholdt ML, Wiebe B, Jespersen SK, Hansen LK, Sillesen H (1998) Quantitative analysis of ultrasound B-mode images of carotid atherosclerotic plaque: correlation with visual classification and histological examination. IEEE Trans Med Imaging 17(6):910–922
45. Xiaohui H, Bruce C, Pislaru C, Greenleaf JF (2000) A novel region growing method for segmenting ultrasound images. IEEE Ultrason Symp 2:1717–1720
46. Xu C, Prince JL (1998) Snakes, shapes and gradient vector flow. IEEE Trans Image Process 7(3):359–369
47. Yu Y, Acton ST (2002) Speckle reducing anisotropic diffusion. IEEE Trans Image Process 11(11):1260–1270
48. Zhang YJ (1996) A survey on evaluation methods for image segmentation. Pattern Recognit 29:1335–1346